Preparation, Structural Development, and Mechanical Properties of Microfibrillar Composite Materials Based on Polyethylene/Polyamide 6 Oriented Blends

Nadya Dencheva, M. Jovita Oliveira, Olga S. Carneiro, António S. Pouzada, Zlatan Denchev

Institute for Polymers and Composites, University of Minho, Campus Azurém, Guimarães 4800-058, Portugal

Received 25 March 2009; accepted 30 August 2009
DOI 10.1002/app.31389
Published online 26 October 2009 in Wiley InterScience (www.interscience.wiley.com).

ABSTRACT: The preparation of microfibrillar composites (MFCs) based on oriented blends of polyamide 6 (PA6) and high-density polyethylene (HDPE) is described. By means of conventional processing techniques, the PA6 phase was transformed *in situ* into fibrils with diameters in the upper nanometer range embedded in an isotropic HDPE matrix. Three different composite materials were prepared through the variation of the HDPE/PA6 ratio with and without a compatibilizer: MFCs reinforced by long PA6 fibrils arranged as a unidirectional ply; MFCs containing middle-length, randomly distributed reinforcing PA6 bristles; and a nonoriented PA6-reinforced material in which the PA6 phase was globular. The evolution of the morphology in the reinforcing phase (e.g., its visible diameter, length, and aspect ratio) was followed during the various processing stages as a function of the blend composition by means of scanning electron microscopy. Synchrotron X-ray scattering was used to characterize selected unidirectional ply composites. The presence of transcrystalline HDPE was demonstrated in the shell of the reinforcing PA6 fibrils of the final MFCs. The impact of the compatibilizer content on the average diameter and length of the fibrils was assessed. The influence of the reinforcing phase on the tensile strength and Young's modulus of the various composites was also evaluated. © 2009 Wiley Periodicals, Inc. J Appl Polym Sci 115: 2918–2932, 2010

Key words: composites; electron microscopy; extrusion; structure-property relations; X-ray

INTRODUCTION

High-density polyethylene (HDPE) and polyamide 6 (PA6) constitute a significant percentage of the most frequently used polymer materials and form a great deal of polymer waste. Therefore, the recycling of HDPE/PA6 blends into useful materials without the costly and time-consuming stage of waste separation is of interest in engineering. A possible solution in this context could be a new group of polymer materials introduced more than a decade ago, which became known as microfibrillar composites (MFCs).[1–3] They combine the lower cost and easier processability of conventional polymer composites with the good mechanical properties of nanostructured composites. In MFCs, both the matrix and reinforcements are obtained *in situ* by a combination of appropriate mechanical and thermal treatments in three processing stages: (1) melt blending of the starting neat polymers and extrusion; (2) cold drawing of the blend; and (3) selective isotropization of the oriented blend at $T_1 < T < T_2$, where T is the temperature, T_1 is the melting temperature of the lower melting component, and T_2 is the melting temperature of the higher melting one.[4] The typical diameters of the reinforcing fibrils in MFCs are within the upper size limit of nanocomposites (i.e., 100–1000 nm), so they can also be regarded as nanostructured polymer composites, although they do not belong among the typical representatives of macrocomposites or nanocomposites.[5]

There are a number of publications on MFC processing, properties, and morphology.[6] In the first studies, the composites were prepared on a laboratory scale, with every one of the three processing stages performed separately, one after another.[1–3,7–11] This discontinuous scheme is difficult to apply in large-scale production. More relevant in this case are the semicontinuous setups developed more recently.[12–14] The blending of the components and their shaping into oriented precursors can be performed in a twin-screw extruder coupled with one or more stretching devices. The selective isotropization of these precursors is performed by compression molding. If they are

Correspondence to: Z. Denchev (denchev@dep.uminho.pt).
Contract grant sponsor: European Commission; contract grant number: HPRI-CT-2001-00140.
Contract grant sponsor: Hamburger Synchrotronstrahlungslabor; contract grant number: II-07-011 EC.
Contract grant sponsor: Fundação para a Ciência e a Tecnologia; contract grant numbers: POCI/CTM/57358/2005, and SFRH/BD/13435/2003 (to N.D. for Ph.D. research).

TABLE I
Basic Characteristics of the Materials

Polymer type	Trade name (manufacturer)	Characteristics
HDPE	VS4531 (Borealis)	Density: 0.94 g/cm^3 Melt flow index: 0.6 g/10 min (2.16 kg/190°C) Complex viscosity: 810 kPa s Melting point: 133°C (DSC)
PA6 (medium-viscosity, general-purpose grade)	Durethan B30 S (Lanxees)	Density: 1.14 g/cm^3 Melt flow rate: 110 cm^3/10 min Viscosity: medium Melting point: 220°C (DSC)
Poly(ethylene-*co*-maleic anhydride) random copolymer (YP)	Yparex 8102 (DSM)	Bound MA: 0.5–1.0% Melt flow index: 2.3 g/10 min (2.16 kg/190°C) M_w: 120.000 M_n: 15.000 Melting point: 125°C

MA = maleic anhydirde; M_n = number-average molecular weight; M_w = weight-average molecular weight.

chopped into pellets, the precursors can be reprocessed by a second extrusion process or by injection molding at a temperature below the melting point of the reinforcing phase. This alternative was reported for the first time by Monticciolo et al.[15] and was applied later by Pesneau et al.,[16] Evstatiev et al.,[17] and Li et al.[18,19] with different polymer blends.

In terms of composition, among the MFCs containing polyolefins, the most studied are the poly(ethylene terephthalate)-reinforced HDPE,[20] polypropylene (PP),[14,21,22] and low-density polyyethylene.[13] HDPE/PA12 MFCs have been obtained and characterized recently.[23] Some HDPE/PA6 composites have also been prepared without a detailed study of the structure or its relationship with the mechanical properties.[24]

The main goals of this study were to obtain MFCs from compatibilized and noncompatibilized HDPE/PA6 blends and optimize the amounts of the PA6 and compatibilizer to achieve superior mechanical properties. Furthermore, the structural development during processing was investigated in MFCs with uniaxially aligned reinforcing fibrils, and the formation of a transcrystalline layer (TCL) at the matrix/fibril interface was proved. An attempt was made to relate the mechanical behavior to the size of the reinforcing fibrils and the TCL that was formed. Scanning electron microscopy (SEM), synchrotron small-angle X-ray scattering (SAXS), and synchrotron wide-angle X-ray scattering (WAXS) techniques were employed in the structural studies.

EXPERIMENTAL

Materials

Table I summarizes the basic properties of the materials used in this study. Before melt mixing and extrusion, PA6 was dried at 90–100°C for 6 h. The HDPE neat polymer and the Yparex compatibilizer (YP) were used as received. As shown in Scheme 1, YP is a maleic anhydride (MAH)/HDPE copolymer with a relatively low concentration of anhydride groups. The effect of *in situ* compatibilization in blends of polyamides and MAH-containing polymers is caused by the chemical reaction between MAH and amine groups from polyamides, which leads to chain scission and the formation of imide linkages. These phenomena have been systematically investigated by several authors[25,26] at temperatures close to those used in this study.

Preparation of the MFC precursors

HDPE, PA6, and YP granules were premixed in a tumbler in the following proportions (wt %): 90/10/0, 80/20/0, 77.5/20/2.5, 75/20/5, 70/20/10, and 65/30/5 HDPE/PA6/YP. Each mixture was introduced into a K-Tron Soder gravimetric feeder (K-Tron International, Inc., Pitman, NJ) that fed it into the hopper of a Leistritz LSM 30.34 laboratory (Leistritz Produktionstechnik GmbH, Nuerenberg, Germany), modular, intermeshing, corotating twin-screw

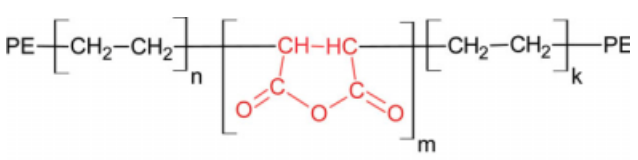

$(n + k)/m \approx 500$

Scheme 1 Chemical structure of YP. [Color figure can be viewed in the online issue, which is available at www.interscience.wiley.com.]

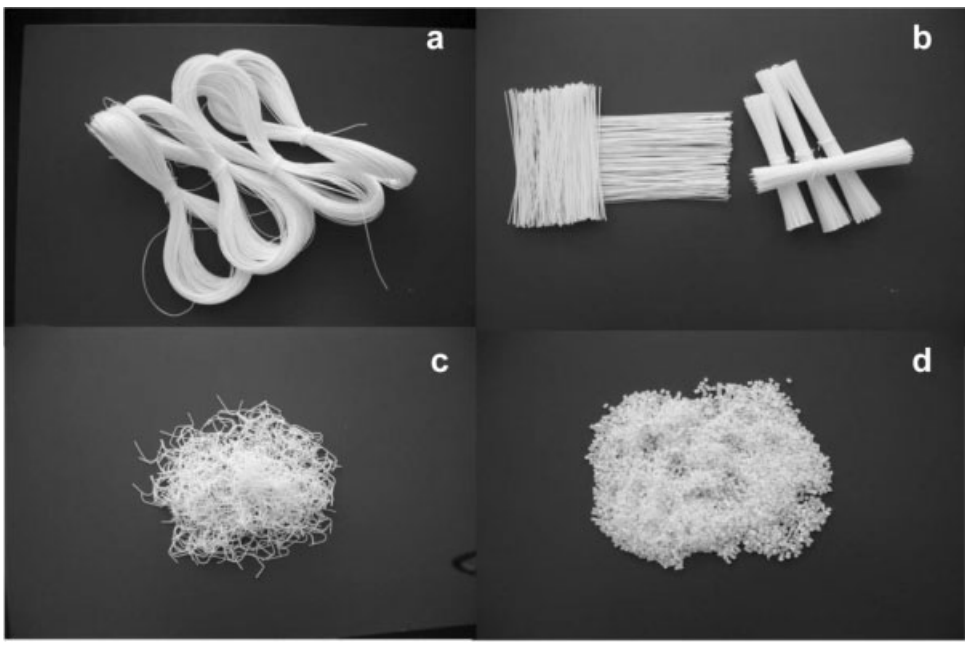

Figure 1 Various MFC precursors obtained after the homogenization and cold-drawing stages: (a) oriented, continuous cables; (b) bundles of cut parallel bristles; (c) MRBs; and (d) nonoriented granules obtained by pelletization after the extruder die.

extruder. The extruder screws rotated at 100 rpm, and the temperature in its 8 sections was set in the range of 240–250°C. The resulting extrudate strand was cooled in the first water bath at 12°C. Meanwhile, the first haul-off unit applied a slight drawing to stabilize the strand cross section. Further drawing was performed in the second haul-off unit after the strand passed through the second water bath heated to 97–99°C. A third haul-off unit applied the last drawing, causing the diameters to decrease from 2 mm (at the extruder die) to approximately 0.6–0.9 mm at the end of the extruder line. Figure 1(a–d) shows all precursors. At the exit of the last haul-off device, the blends were in the form of oriented, continuous cables, which were the basic precursors for the preparation of the MFCs by compression molding. The oriented, continuous cables could be used, after adequate cutting and alignment, in the form of unidirectionally arranged bundles [unidirectional plies (UDPs)] or middle-length, randomly oriented bristles (MRBs). For comparison, nonoriented granules obtained by the pelletization of each extrudate after the extruder die were also produced and hot-pressed to obtain the reference nonoriented material (NOM).

Preparation of the final MFCs

Each precursor type was subjected to selective melting, by which isotropization and controlled crystallization of the matrix occurred in a hot press at a fixed temperature of 160°C, a pressure of 2 MPa, and a cooling rate of about 10°C/min. Standard rectangular laminate plates (60×120 mm^2 with a thickness of 0.1–1.5 mm) were obtained from all the precursors. They were used for structural and morphological characterization and to yield specimens for the tensile tests.

SEM

To analyze the morphology of the MFCs and their precursors, freeze-fractured specimens were studied with SEM. For each blend, specimens were collected for morphological analysis, typically at three different locations of the extruder line: at the extrusion die, after the first haul-off unit, and after the second haul-off unit. The final MFCs obtained after compression molding were also analyzed. All samples were sputter-coated with gold and observed with a Leica S360 scanning electron microscope (Leica Microsystems Cambridge Ltd., Cambridge, UK) at magnifications of 2000, 5000, and 7500×. Most of the studied specimens were obtained by cryogenic fracturing with liquid nitrogen, and the fractured surfaces were observed with SEM. The oriented, continuous cables obtained after the second haul-off unit, as well as some nonoriented precursors (as specified further), were observed with the same technique after selective extraction of the polyethylene (PE) matrix with hot toluene for 5 h.

Mechanical tests

The tensile tests were performed with an Instron model 4505 tensile testing machine (Instron, High

Wycomb, UK). The tests were carried out at 23 ± 2°C with a standard load cell of 1 kN at a constant crosshead speed of 50 mm/min. From the compression-molded plates obtained with different precursors (UDP, MRB, or NOM), specimens for tensile tests were cut out with a gauge length of 25 mm and a width of 4 mm. The sample thickness varied in the range of 1.0–1.5 mm. At least five specimens of each sample were studied to calculate the average and standard deviation values. The engineering stress was determined as the ratio of the tensile force to the initial cross section of the sample. The engineering strain was determined as the ratio of the sample gauge length at any time during drawing to that before drawing. The stiffness was calculated as the secant modulus from the stress–strain curves at 1% strain.

X-ray scattering techniques

All WAXS and SAXS patterns in this study were registered at the Soft Condensed Matter Beamline (A2) of the Hamburger Synchrotronstrahlungslabor (Hamburg, Germany) with synchrotron radiation with the wavelength fixed at 0.15 nm. The sample-to-detector distance for SAXS was set at 2830 mm, the diffraction patterns being registered with an MAR charged coupling device, two-dimensional (2D) detector with an exposure time of 30 s. For the WAXS measurements, the detector was positioned at 90 mm with respect to the sample. The various MFCs were studied in the transmission mode, the sample thickness being in the range of 1.0–1.5 mm. Scattering patterns were obtained at certain temperatures at a typical heating rate of 20°C/min. A specially designed sample holder was used to allow controlled heating/cooling of the sample in the range of 25–300°C. An Imago multichannel process and program controller from Jumo GmbH & Co. KG (Fulda, Germany) was used to regulate the sample temperature during heating or cooling at various rates. The difference between the readout and real temperature of the sample was found to be 3–4°C at a heating or cooling rate of 20°C/min.

RESULTS AND DISCUSSION

SEM investigations

Figure 2 displays selected SEM images of PA6-containing materials at different stages of the MFC processing: the MFC after the extruder die (column 1), the MFC after the first haul-off unit (column 2), and the final MFC in the form of UDP (column 3). To observe the reinforcing fibrils, the specimens were cut in such a way that the fracture plane was parallel to the fibril axis.

Figure 2(6c) presents the MFC containing the maximum amount of PA6. This sample was impossible to fracture like all the others. Thus, the observation of fibrils by SEM was possible only after selective dissolution of the HDPE matrix in hot toluene for 5 h. Because of the removal of the matrix, the reinforcing fibrils lost their original parallel alignment in the composite.

As shown in Figure 2, in the samples without YP [Fig. 2(1a,2a)], immediately after the extruder die, the PA6 phase was well dispersed in globular domains (nodules) with average diameters of 3–4 μm. In the presence of YP [Fig. 2(3a–5a)], the diameter of the globules became significantly smaller (ca. 1.5 μm); that is, the higher the compatibilizer concentration was, the smaller the PA6 nodules were. Such a well-expressed reduction of the size of the dispersed phase was observed earlier and recognized as an indication for the grafting of PA6 onto the MAH-containing compatribilizer.[25] An additional effect of the compatibilizer, evident from the SEM images, was the narrower size distribution of the reinforcing phase within the HDPE matrix. In the system with 30% PA6 [Fig. 2(6a)], the diameters of the PA6 droplets reached the highest value, about 4.5 μm. This may have been due to the unfavorable combination of a high PA6 concentration with a low amount of the compatibilizer, which prevented good mixing of the system. As expected, after the first haul-off unit [Fig. 2(1b–6b)], the diameter of the polyamide entities decreased up to 3.5 times because of their stretching.

The SEM images of the final MFCs [Fig. 2(1c–6c)] deserve special attention. The SEM method undoubtedly confirmed that (1) the PA6 reinforcing phase had a well-expressed fibrillar morphology and (2) the average diameters of these fibrils were in the upper nanometer to lower micrometer range (e.g., between 700 and 1000 nm).

None of the images of MFCs in Figure 2 permitted us to measure the fibril length directly. Indirectly, the average lengths and aspect ratios of the reinforcing PA6 fibrils could be evaluated after some simplifying suppositions were made. The micrographs show that at the extruder die (i.e., in the absence of orientation), the PA6 entities were globular [Fig. 2(1a–6a)]. After the diameters of these globules were measured, the average volume of the spherical PA6 entities could be calculated. Furthermore, the diameters of the fibrils in the final MFCs were measured from Figure 2(1c–6c) and were averaged. Under the assumption that the fibril geometry was cylindrical and that the fibrils were produced by the deformation of the respective PA6 spherical nodules without the formation of voids (i.e., the volumes of the PA6 spheres at the extruder die and of the MFC fibrils were the same), we could estimate the average

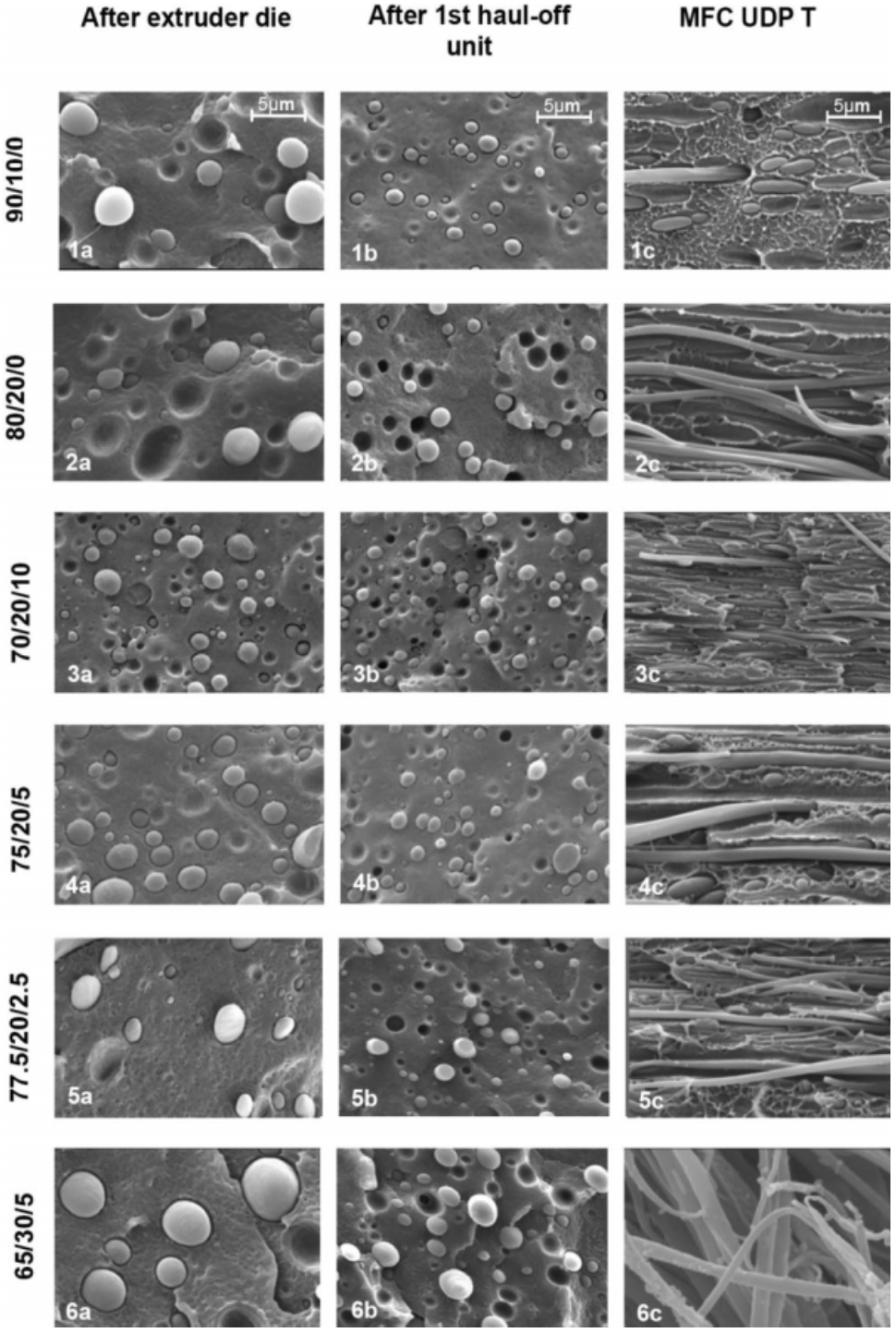

Figure 2 SEM images of HDPE/PA6/YP surfaces after cryogenic fracturing during the various stages of MFC preparation (compositions are given as weight percentages): (1a–6a) the nonoriented blend right after the extruder die, (1b–6b) the slightly oriented blends after the first haul-off unit, (1c–5c) the UDP composites fractured along the fibril axis, and (6c) the 65/30/5 UDP composite after selective extraction of the HDPE matrix.

length of the fibrils and therefore the aspect ratio (Table II). Thus, in noncompatibilized PA6-reinforced MFCs, the calculated length of the reinforcing fibrils was up to 51 μm, whereas the maximum length in the MFCs containing 20% PA6 in the presence of the compatibilizer was 5–25 μm. Keeping in mind the variation of the fibril diameters, we could estimate the aspect ratio (Table II). It can be seen that the noncompatibilized 80/20/0 sample and the sample with 30% PA6 showed the highest maximum aspect ratios, which went down gradually as the YP content was increased.

TABLE II
Dimensions of the PA6 Reinforcing Phase in Various HDPE/PA6/YP Materials as Revealed by SEM Measurements

HDPE/PA6/YP composition (wt %)	Diameter of the PA6 nodules at the extruder die (nm)	Dimensions of the PA6 fibrils after the first haul-off unit (nm)			Dimensions of the PA6 fibrils in the UDP MFC (nm)		
		Average diameter	Estimated length	Maximum aspect ratio	Average diameter	Estimated length	Maximum aspect ratio
90/10/0	3,500	1,200	19,850	16.5	1,000	28,600	28.6
80/20/0	3,500	1,000	28,600	28.6	750 (570)	50,815 (87,668)	67.8 (153.5)
70/20/10	1,500	500	9,000	18	700 (714)	4,592 (4,414)	6.6 (6.2)
75/20/5	2,000	1,250	3,413	2.7	800	8,333	10.4
77.5/20/2.5	2,750	1,250	8,873	7.1	750	24,650	33.0
65/30/5	4,500	1,500	27,000	18	1,000	60,750	60.8

The values in parentheses are for oriented blends after the selective extraction of the HDPE matrix.

Figure 3 shows micrographs of the composites produced from different precursors. The influence of the alignment of the reinforcing phase on the morphology could be seen in two representative MFCs: one without the compatibilizer (80/20/0) and one with a 10% concentration of the compatibilizer (70/20/10).

In UDPs, all the fibrils lay nearly parallel to the fracture plane [Fig. 3(1a,1b)]. Figure 3(2a,2b) presents composites produced from MRBs. There, a great variety of fibril cross-section shapes can be seen (rectangular, circular, or oval), depending on the angle between the fibril and the fracture plane. In the NOM samples [Fig. 3(3a,3b)], however, only oval-shaped entities instead of fibrils were observed, and this indicated that after the extruder die, the orientation of the PA6 component was either absent or very low. It is also interesting to observe in the images of Figure 3 the improvement in the adhesion between PA6 and HDPE in the presence of the compatibilizer. This effect is particularly clear when Figure 3(1a) and Figure 3(1b) are compared. In the absence of YP (first image), the fibrils were completely detached from the matrix, whereas in the specimen with the compatibilizer (second image), they were well embedded, evidencing good adhesion.

As previously confirmed,[24,25] the copolymer that formed between the PA6 fibril material and the MAH linkages of YP acted like a bridge between the HDPE matrix and the reinforcing PA6, thus strengthening the interface. It was interesting to check how the fibrils looked after the selective removal of the HDPE matrix material in the MFCs prepared without YP [Fig. 4(1a)] and with YP at a 10 or 5% concentration [Fig. 4(2a,3a)]. The extraction was performed with hot toluene, and the duration was kept the same for all the samples

Apparently, in the absence of the compatibilizer [Fig. 4(1a)], the HDPE matrix was easier to dissolve and remove, the remaining fibrils being quite smooth. In the presence of 10% YP and after extraction, the fibrils were still covered by many globular fragments, most likely originating from the isotropic matrix. Increasing the PA6 content up to 30% and decreasing the percentage of YP [Fig. 4(3a)] produced smooth fibrils similar to those when no compatibilizer was applied. It can be supposed that the fibril roughness in Figure 4 is related to the HDPE–PA6 copolymer, which is expected to be less soluble in toluene because of the inclusion of PA6 segments.

Figure 4 also shows that after the die exit [Fig. 4(1b,3b)], the reinforcing phase was globular, and the linkage at the PA6/HDPE interface appeared to be stronger in comparison with the fibril reinforcements [Fig. 4(1a–3a)]. The fibril thicknesses in the

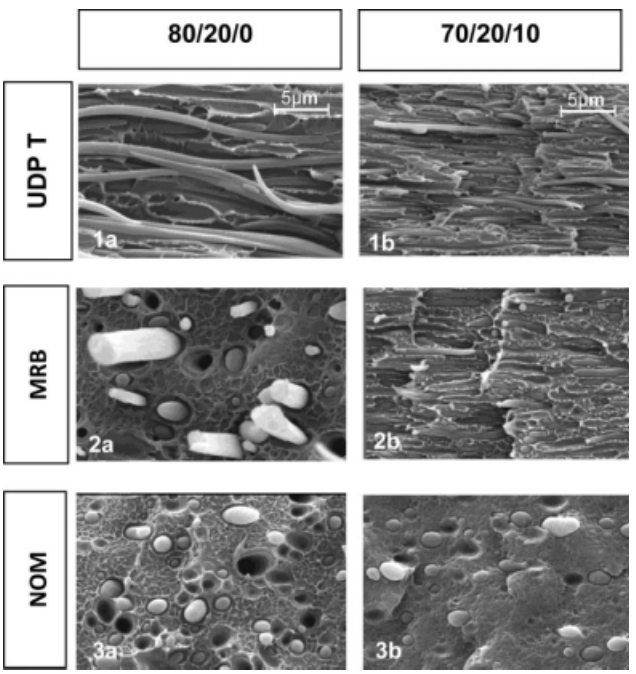

Figure 3 SEM images of the surfaces (after cryogenic fracturing) of MFCs made from two HDPE/PA6/YP blends: (a) 80/20/0 and (b) 70/20/10 wt %. MRB indicates a composite from middle-length PA6 bristles with a random orientation, NOM indicates a material obtained from nonoriented granules of the two blends, and UDP T indicates a unidirectional ply fractured parallel to the fibril direction.

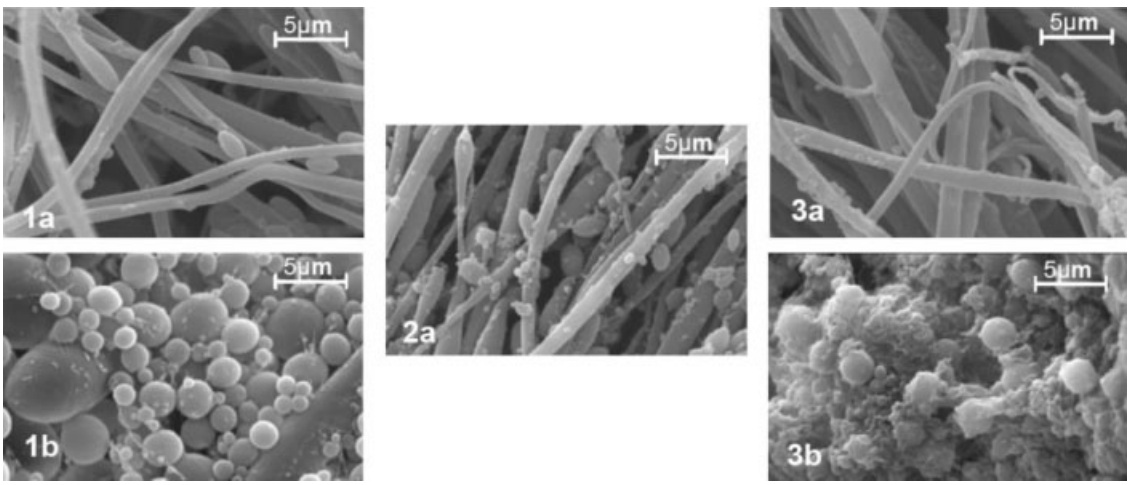

Figure 4 SEM images of HDPE/PA6/YP samples (after the extraction of the matrix) with compositions of (1) 80/20/0, (2) 70/20/10, and (3) 65/30/5 wt %: (a) the final MFCs and (b) NOM after the die exit.

latter images were quite similar, regardless of the sample composition.

Another interesting observation can be made from a comparison of Table II and Figure 4. With the 80/20/0 sample, the selective extraction of the HDPE matrix material led to a drastic increase in the aspect ratio (from ca. 68 to 154), whereas in the 70/20/10 sample containing the maximum amount of YP, the aspect ratio remained unchanged. This was an indirect indication that the reinforcing fibrils observed by SEM most likely contained a core of PA6 and a shell of HDPE, the latter being chemically bonded to the core in the MFCs containing YP or only physically attached to it in the noncompatibilized samples. This phenomenon was further studied with SAXS and WAXS.

Tensile properties of HDPE/PA6/YP UDP

Because the UDP lamina represents the basic building block of long-fiber-reinforced composites,[27] tensile tests were performed on laminae produced from HDPE/PA6/YP composites with various compositions. Test samples were cut out along the longitudinal axis of the orientation. Typical stress–strain curves of various UDP MFCs are shown in Figure 5.

The 90/10/0 composition containing 10 wt % PA6 (curve 1) displayed ductile behavior similar to that of the HDPE matrix. In both curves, clear yielding and necking can be seen, even though the strain at break of the composite (ca. 100%) was much lower than that of HDPE (ca. 800%). The other stress–strain curves have the typical brittle shape of composite materials, the strain at break not exceeding 30–40% and the ultimate tensile stress being considerably higher than that of the matrix.

Based on the stress–strain curves of each series, the longitudinal modulus was determined as the secant modulus at 1% strain, and the data are summarized in Table III. The same table also presents data for the longitudinal tensile strength (σ_{max}, which is defined as the maximum stress that a material can withstand) and the longitudinal yield stress (σ_y). For specimens without pronounced yielding, $\sigma_y \equiv \sigma_{max}$. All MFC compositions showed improved moduli in comparison with HDPE. The improvements were in the 11–33% range, the biggest improvement being for the composites without the compatibilizer and the smallest being for the composition with 10% YP.

The yield stress and tensile strength of all the UDP composites grew significantly, from 26 MPa for HDPE to more than 60 MPa for the 80/20/0 MFC composition. Again, the MFC with the highest concentration of the compatibilizer showed the smallest enhancement of the tensile properties. The most

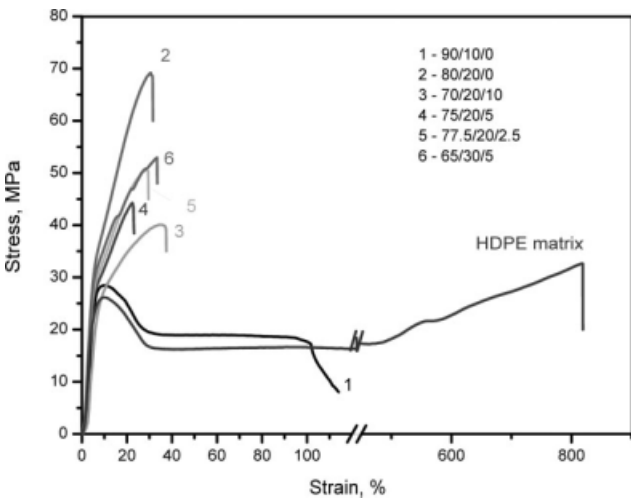

Figure 5 Typical stress–strain curves of HDPE/PA6/YP UDP MFCs. For comparison, the curve corresponding to the HDPE matrix is also shown.

TABLE III
Longitudinal Tensile Properties of the HDPE/PA6/YP UDP MFCs with Various Compositions

HDPE/PA6/YP composition (wt %)	Volume fraction of PA6	E (MPa)[a]	ΔE (%)[b]	σ_{max} (MPa)	$\Delta\sigma_{max}$ (%)[c]	σ_y (MPa)
100/0/0	–	827 ± 47	0	26 ± 1	0	26 ± 1
90/10/0	0.084	940 ± 21	13.7	27 ± 1	3.8	27 ± 1
80/20/0	0.171	1095 ± 52	32.4	57 ± 4	119.2	57 ± 4
70/20/10	0.171	920 ± 7	11.2	37 ± 2	42.3	37 ± 2
75/20/5	0.171	961 ± 19	16.2	45 ± 3	73.1	45 ± 3
77.5/20/2.5	0.171	1030 ± 19	24.5	45 ± 3	73.1	45 ± 4
65/30/5	0.261	1098 ± 48	32.8	52 ± 8	100.0	51 ± 9
0/100/0 oriented		1830 ± 31	–	230 ± 7	–	208 ± 7

[a] E was determined as the secant modulus at 1% strain.
[b] $\Delta E = (E_{HDPE} - E)/E_{HDPE}$, where E_{HDPE} is the secant modulus for HDPE at 1% strain.
[c] $\Delta\sigma_{max} = (\sigma_{HDPE} - \sigma)/\sigma_{HDPE}$.

plausible explanation for these results is related to the strong decrease in the aspect ratio of the reinforcing PA6 fibrils as the YP concentration increased (Table II). Considering the character of the chemical reaction between YP (representing an MAH-*g*-PE copolymer) and PA6,[25] we can suppose that the aspect ratio dropped because of some degradation that took place in the PA6 phase during the melt blending and mostly during the selective isotropization.

Another explanation for the observed deterioration of the mechanical properties of the HDPE/PA6 blends in the presence of the MAH-*g*-PP copolymer is related to the low molecular weight of the copolymer compatibilizer, which produces adhesion between the two polymer phases but also acts as a mechanically weak boundary layer between them, propagating the formation of cracks in the presence of external stress.[28]

Influence of the alignment of the reinforcement on the tensile behavior

The influence of the fibril alignment on the tensile behavior was evaluated by a comparison of the mechanical properties of the UDP laminae with those of the composites from MRB precursors. To assess the role of the fibrillar reinforcement, composites containing a nonoriented, globular PA6 phase (NOM) were also studied.

The secant moduli of these materials as a function of their composition are compared in Figure 6. All the composites types, regardless of the orientation and alignment of the PA6 phase, displayed secant moduli higher than that of HDPE, the only exception being the 65/30/5 system, in which only the UDP lamina showed improved tensile stiffness.

In the case of the 90/10/0 composites, there was no statistically significant difference between the moduli of UDP, MRB, and NOM; that is, the type of PA6 reinforcement (fibrillar or isotropic) and the alignment of the fibrils did not influence the stiffness. Considering the compositions with 20% PA6, we could assess the influence of these two parameters as well as that of the compatibilizer. Clear enhancement in the modulus existed only when the reinforcements were aligned fibrils in the UDP laminae. Within the series with 20% PA6, high moduli were achieved either without or with low compatibilizer concentrations (e.g., the 80/20/0 UDP and 77.5/20/2.5 UDP systems). When the reinforcing component was isotropic (NOM), the trend in the 20% PA6 series was inversed. In this case (e.g., the 70/20/10 NOM system), the higher compatibilizer concentration favored the stiffness. Apparently, the compatibilizer positively affected the mechanical properties whenever the PA6 reinforcement was isotropic. This was in good agreement with the observations of the SEM morphological study of various precursors after selective dissolution of HDPE (Fig. 4). The matrix was removed much more easily in the oriented precursors, and this left smoother fibrils [Fig. 4(1a–3a)].

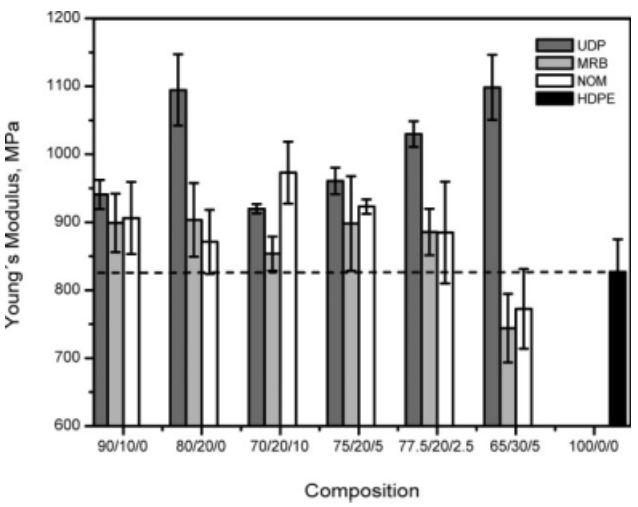

Figure 6 Longitudinal secant modulus of the HDPE/PA6/YP UDP, MRB, and NOM composites and the HDPE matrix.

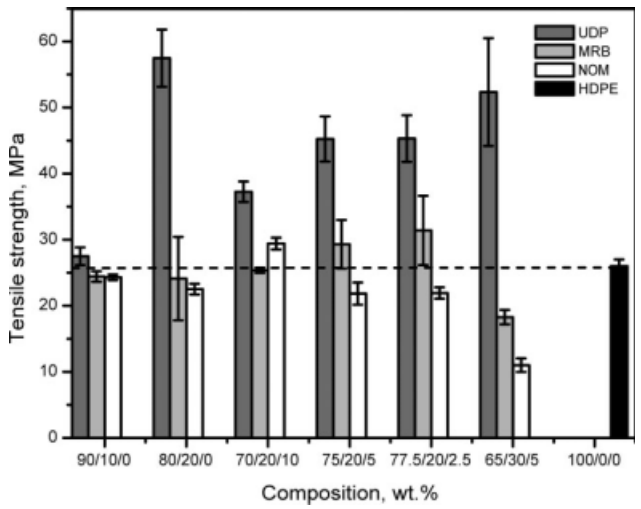

Figure 7 Longitudinal tensile strength of the HDPE/PA6/YP UDP, MRB, and NOM composites and the HDPE matrix.

As far as the tensile strength is concerned (Fig. 7), a clear increase in the σ_{max} values was observed only in the UDP MFCs, that is, those with aligned fibrillar reinforcement. The influence of the compatibilizer concentration was similar to that in the case of stiffness: the higher the YP content was, the lower the strength was. The 80/20/0 system without the compatibilizer showed an improvement in σ_{max} of about 120%.

In the isotropic MRB and NOM composites, the tensile strength data were close to or even worse than those of the matrix. It can be concluded that what improved the mechanical properties of the HDPE matrix was not the mere presence of the stronger PA6 phase but rather the nanostructured PA6 fibrils with a high aspect ratio. Thus, to get *in situ* MFCs of higher strength and stiffness in not only one direction, one should consider the preparation of laminates with several UDPs aligned differently.

2D SAXS studies of HDPE/PA6/YP MFC

Figure 8 presents SAXS patterns of two HDPE/PA6/YP UDP MFC compositions, one without the compatibilizer (80/20/0) and one with the compatibilizer (70/20/10), at different temperatures. The first examination of the 2D SAXS patterns [Fig. 8(1a,2a)] showed that both composites contained isotropic scattering of randomly distributed lamellar structures and equatorial scattering maxima attributable to lamellar crystals oriented parallel to the horizontal fiber direction. The isotropic ring and the oriented maxima displayed similar long spacings greater than 220 Å. This was a clear indication that the observed oriented reflections could not have originated from the reinforcing PA6 phase, whose long spacings are typically between 70 and 90 Å.[29] Consequently, it can be supposed that a fraction of the HDPE matrix material crystallized on the oriented PA6 fibrils, thus forming a TCL at the interface.

Without a special treatment, it was impossible to observe at the same time the HDPE and PA6 scattering in Figure 8(1a,2a) because of the strong differences in the scattering intensities. Heating the two UDP MFC samples at 160°C eliminated the HDPE scattering and revealed the oriented PA6 reflections [Fig. 8(1b,2b)]. Cooling to 30°C caused the HDPE matrix to recrystallize. This process took place differently in the two MFCs under investigation.

The oriented HDPE TCL in the 70/20/10 MFC at 30°C after the selective melting of the matrix maintained its equatorial orientation [Fig. 8(2c)], whereas in the 80/20/0 system, it rotated by 90° and appeared at the meridian [Fig. 8(1c)]. Isotropic scattering was also present in the two patterns.

This reorientation of the HDPE scattering was better observed when azimuthal cuts of the aforementioned patterns were performed (Fig. 9).

The curve of the noncompatibilized sample [Fig. 9(a)] clearly shows that after recrystallization, the peak of the intensity was not at 0° (i.e., along the fiber axis) but was at −90 or 90°. In the compatibilized sample [Fig. 9(b)], the azimuthal distribution of the scattered intensity remained the same at 30°C and at 30°C after 160°C. It is noteworthy that this reorientation of the lamellae that took place in the noncompatibilized samples was not accompanied by chain direction reorientation; that is, the chain direction of PA6 and that of the oriented HDPE fraction continued to coincide, as in the starting image at 30°C. This effect is discussed in the next section, which is dedicated to the WAXS studies.

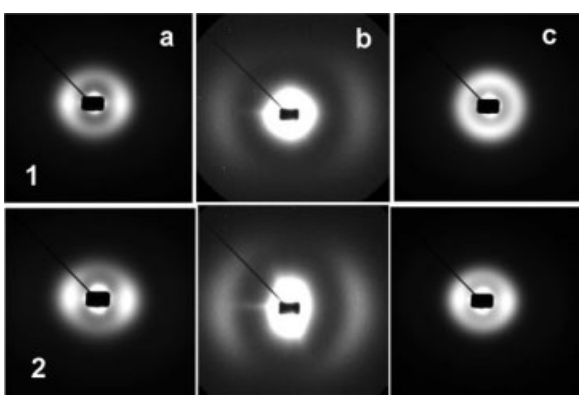

Figure 8 2D SAXS images of two HDPE/PA6/YP UDP MFC with compositions of (1) 80/20/0 and (2) 70/20/10 at different temperatures: (a) the pattern of the starting MFC at 30°C, (b) the pattern at 160°C with heating in the beam, and (c) the pattern at 30°C after heating at 160°C. The fibril axis is horizontal.

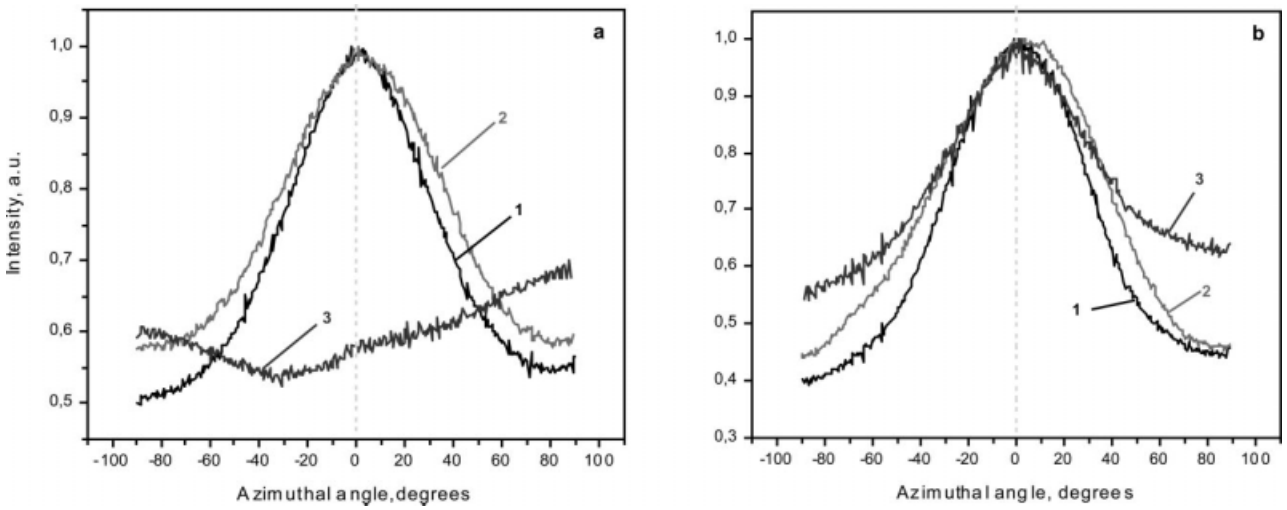

Figure 9 Azimuthal distribution of the scattered intensity in the 2D SAXS images of two HDPE/PA6/YP UDP MFCs with compositions of (a) 80/20/0 and (b) 70/20/10: (1) the initial MFC at 30°C, (2) the MFC with beam heating at 160°C, and (3) the MFC at 30°C after heating to 160°C. The dashed line indicates the fiber direction.

To make a distinction between the two fractions of HDPE, the subtraction procedure described by Somani et al.[30] was used. The 2D SAXS patterns were first corrected for the incident beam intensity, and then the empty chamber scattering was subtracted. It was assumed that the total scattered intensity could be separated into two contributions: (1) the isotropic contribution from the amorphous chains and the nonoriented crystals, which was directly proportional to the azimuthally independent component of the total scattered intensity, and (2) the oriented contribution from all oriented scatterers (with various degree of orientation), which was calculated by subtraction of the azimuthally independent component from the total scattered intensity. To determine the azimuthally independent intensity and to perform the subtraction, a subroutine incorporated into Polar 2.7.1 X-ray software was used.[31] Thus, Figure 10(a) shows the pattern of the total scattering of the 75/20/5 UDP MFC composition at 30°C. The computer-generated 2D image of the isotropic intensity is presented in Figure 10(b), and the resulting image (obtained after the subtraction of part b from part a) corresponding to the oriented scattering is shown in Figure 10(c). As the latter shows, the procedure not only separated the two HDPE components but also revealed clearly the oriented PA6 fraction located along the equator.

In Figure 11, three-dimensional (3D) visualization of the initial pattern [Fig. 11(a)] and the oriented scattering [Fig. 11(b)] for the same 75/20/5 composition is presented. Figure 11(b) better shows the PA6 contribution to the oriented part of the scattering, which is indicated by arrows.

Table IV presents the HDPE and PA6 long-spacing values determined from the scattering patterns of six UDP MFCs with different HDPE/PA6/YP compositions. In the absence of the compatibilizer, there were no significant differences between the long spacings of HDPE lamellae located in the bulk (isotropic) and those of the oriented HDPE lamellae in the TCL (oriented). Introducing YP resulted in smaller long periods in the oriented HDPE fraction, whereas those of the bulk matrix fraction remained like those in the noncompatibilized compositions. Only in the 65/30/5 UDP MFC was the distance between the oriented HDPE lamellae greater than that of the isotropic fraction. Most likely, this could be explained as a result of the larger amount of PA6 in this composition. With respect to the PA6 long-spacing values, they varied in the range of 77–95 Å. The PA6 long period of 77 Å in the 65/30/5 composition was the closest to the value of the oriented neat PA6.[29]

As mentioned previously, after recrystallization, the HDPE fraction in the noncompatibilized and compatibilized samples oriented in different ways; in the first case, the scattering maxima appeared on the meridian, whereas in the second, they

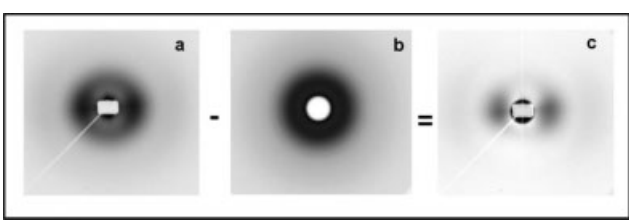

Figure 10 Deconvolution procedure of the SAXS pattern of the 75/20/5 UDP MFC: (a) the original SAXS image, (b) the intensity pattern of the isotropic scattering, and (c) the intensity pattern of the oriented scatterers (obtained by the subtraction of part b from part a). The fiber axis is horizontal.

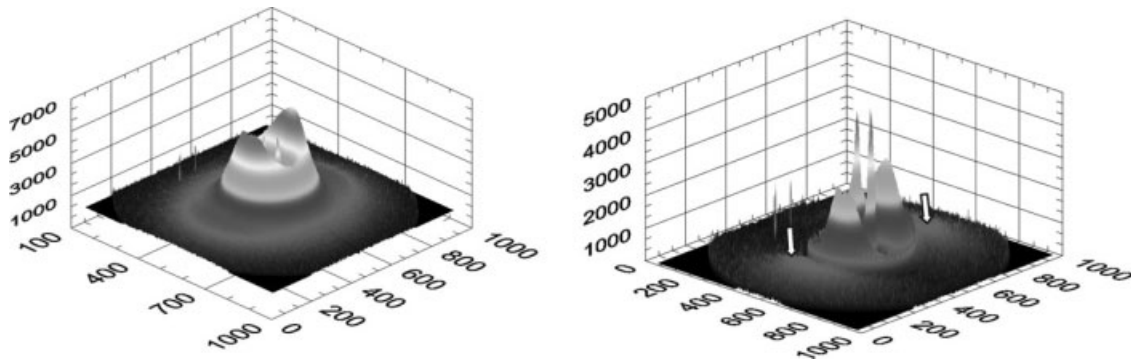

Figure 11 3D SAXS patterns of UDP MFCs before (left) and after (right) the subtraction of the azimuthally independent component of the total scattered intensity. The white arrows indicate the scattering of the PA6 reinforcing phase.

maintained their position on the equator. As shown in Table IV, in both the 80/20/0 and 70/20/10 samples, an increase in the long spacing of isotropic HDPE, in the presence and absence of the compatibilizer, was observed after matrix recrystallization (the data are presented in parentheses).

2D WAXS studies of HDPE/PA6/YP MFC

Both SEM and SAXS studies of UDP MFC materials provided evidence that the reinforcing fibrils most likely had a layered, coaxial structure: a core of oriented PA6 and a shell of oriented, transcrystalline HDPE. The WAXS measurements supported and allowed further development of this hypothesis.

A visual inspection of the 2D WAXS patterns of UDP MFCs (Fig. 12) showed that the crystallographic characteristics of HDPE and PA6 were very similar, and this led to strong overlapping of the respective diffraction peaks. Nevertheless, we can note that at 30°C, there was a coexistence of isotropic Debye rings and crystalline reflections oriented parallel to the horizontal fibril direction. At 160°C, the HDPE reflections changed into a diffuse amorphous halo, revealing the oriented PA6 reflections.

To separate the contributions of the isotropic and oriented crystalline fractions and to study their origins, the same subtraction procedure used with the SAXS patterns was applied. Figure 13 exemplifies this treatment for the 80/20/0 and 70/20/10 HDPE/PA6/YP UDP MFCs, showing the starting real 2D WAXS patterns, the computer-generated isotropic part of the scattered intensity, and the resulting 2D WAXS images of the oriented part after subtraction.

Subtracting the isotropic crystalline and amorphous fractions allowed the outlining of the oriented crystalline reflections, which were otherwise undetectable. Together with the expected oriented PA6 reflections in the right images in Figure 13, we can also observe clear reflections of the oriented matrix. The two weak equatorial arcs belong to the (200) and (002/202) planes of PA6, and the other two, more intense equatorial reflections belong to the (110) and (200) planes of the orthorhombic unit cell of HDPE. This is one more indication for epitaxial crystallization of the matrix material upon the reinforcing fiber, by which the chain direction in the matrix crystals coincided with that in the reinforcing PA6 fibrils. On the basis of Figure 13, this observation was valid for both the noncompatibilized and compatibilized samples.

Figure 14 shows the 3D images of the real WAXS patterns before the treatment and the oriented scattering after subtraction of the same two MFCs. The

TABLE IV
Long-Spacing Values of the HDPE/PA6/YP UDP Composites at 30°C Without (L_B) and With (L_B*) Deconvolution

		L_B (Å)		L_B* (Å)		
Number	HDPE/PA6/YP composition	PA6	Total HDPE	Isotropic HDPE	Oriented HDPE	Oriented PA6
1	90/10/0	100.5	223	224	222	95
2	80/20/0	90	229	225 (231)	222 (225)	86
3	77.5/20/2.5	94	221	224	211	91
4	75/20/5	94	220	224	213	92
5	70/20/10	87	215	225 (245)	210 (214)	88
6	65/30/5	82	236	223	231	77

The values in parentheses were obtained after the recrystallization of HDPE by in-beam heating to 160°C followed by cooling to 30°C.

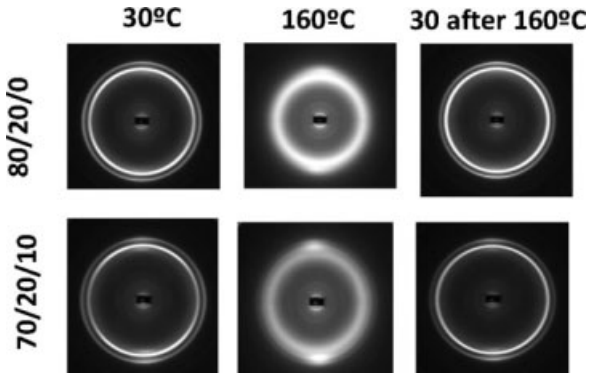

Figure 12 2D WAXS patterns of HDPE/PA6/YP MFCs taken at various temperatures. The fibril direction is horizontal.

white arrows indicate the position of the α-PA6 (200) reflection. This representation better shows the anisotropy of the HDPE (110) and (200) diffractions.

For a quantitative evaluation of the oriented and isotropic parts of the total scattered intensities, the respective 2D WAXS patterns were integrated in the 0–180° range to obtain one-dimensional (1D) WAXS profiles, which were afterwards fitted with Gaussian peaks. The results from peak fitting applied to the 80/20/0 MFC sample are presented in Figure 15(a,b). The deconvolution of the integral profile of the oriented part clearly showed the (110), (200), and (210) contributions of HDPE [Fig. 15(a), shaded reflections] and also the four crystalline reflections of α-PA6 and γ-PA6. The peak fitting of the isotropic part displayed (110), (200), and (210) crystalline reflections of the HDPE matrix only and the amorphous halos of PA6 and HDPE, respectively [Fig. 15(b)]. Based on the angular positions of the reflections, the *d*-spacings of the corresponding planes were calculated. A quantitative evaluation of the

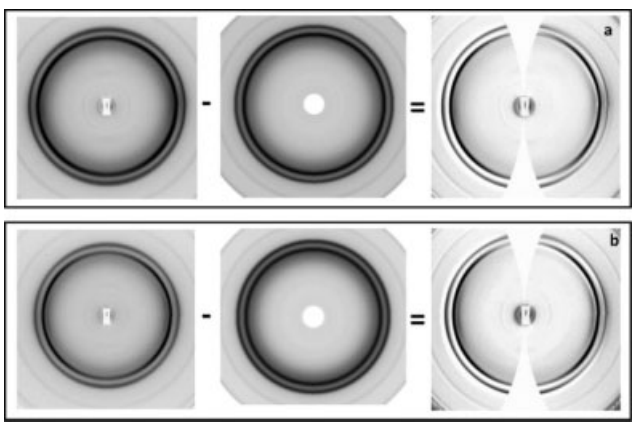

Figure 13 Example of the analysis of the WAXS patterns at 30°C of UDP MFCs with compositions of (a) 80/20/0 and (b) 70/20/10: the total scattered intensity (left), the calculated isotropic intensity (center), and the oriented scattered intensity (right). The fiber axis is vertical.

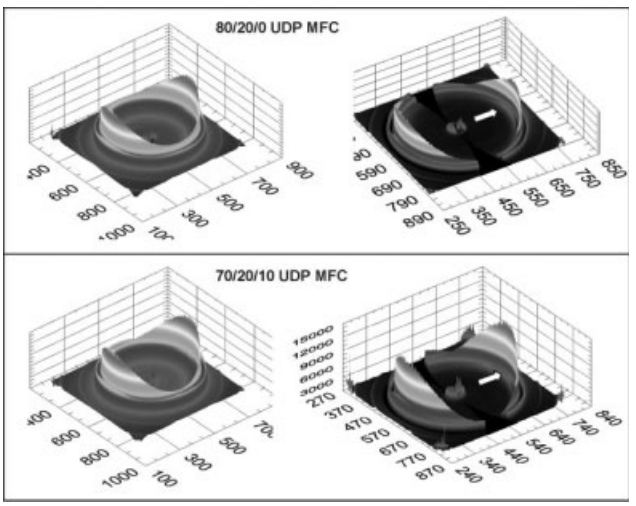

Figure 14 3D WAXS patterns of UDP MFCs before (left) and after (right) the subtraction of the azimuthally independent component of the total scattered intensity. The white arrows point to the (200) reflection of α-PA6.

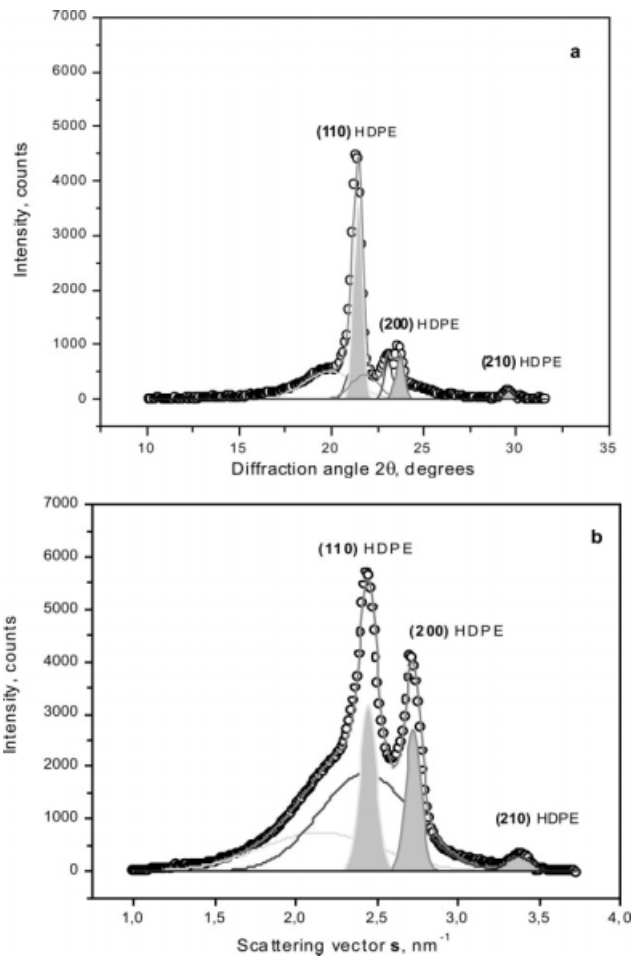

Figure 15 1D WAXS profiles of the 80/20/0 HDPE/PA6/YP UDP MFC exemplifying the peak fitting of (a) the oriented scattering and (b) the isotropic WAXS scattering. The pattern in part a was obtained after the subtraction of part b from the initial WAXS pattern with the total scattered intensity.

TABLE V
Results from the Deconvolution of the Oriented and Isotropic Parts of 2D WAXS Patterns of Selected HDPE/PA6/YP UDP MFCs

	HDPE/PA6/YP					
	80/20/0			70/20/10		
WAXS reflection	2θ (°)	Content (%)	d_{hkl} (Å)	2θ (°)	Content (%)	d_{hkl} (Å)
Oriented part of the WAXS intensity						
(200) : α-PA6	19.90	28.5	4.34	19.92	28.7	4.34
(001) : γ-PA6	21.05	6.6	4.11	21.35	7.6	4.07
(110) : HDPE	21.44	34.9	4.03	21.33	38.2	4.05
(200) : γ-PA6	21.79	13.7	3.97	21.66	7.6	3.99
(002)/(202) : α-PA6	23.09	6.9	3.75	22.99	6.9	3.76
(200) : HDPE	23.69	7.9	3.65	23.74	9.1	3.65
(210) : HDPE	29.61	1.5	2.94	29.50	1.9	2.95
PA6 fraction (%)		55.7			50.8	
HDPE fraction (%)		44.3			49.2	
Isotropic part of the WAXS intensity						
(110) : HDPE	21.13	14.6	4.09	20.97	9.8	4.12
(200) : HDPE	23.56	11.4	3.67	23.48	12.6	3.69
(210) : HDPE	29.29	1.9	2.96	29.24	1.3	2.97

In the isotropic part of the WAXS intensity, only the crystalline reflections are included. The difference from 100% provides the content of the amorphous HDPE and amorphous PA6. d_{hkl} is the *d*-spacing of the respective crystalline plane. The oriented reflections are considered 100% crystalline.

peak-fitting results for two representative MFCs, one without compatibilization (80/20/0) and one with compatibilization (70/20/10), and data for *d*-spacings are given in Table V.

From Figure 15 and Table V, we can see that a significant part of the HDPE matrix was able to crystallize in an oriented fashion along the PA6 fiber, thus forming a TCL in such a way that the chain directions of the two polymers coincided. The rest of the matrix, situated in the bulk, crystallized isotropically. The relation between the content of the PA6 fibrils and the oriented part of the HDPE matrix (the crystalline fraction) was almost 1.03 : 1.00 in the 70/20/10 MFC system and 1.26 : 1.00 in the 80/20/0 system. This meant that in the presence of the compatibilizer, a larger part of the HDPE was included in the TCL without considerable changes in its crystallographic characteristics. On the basis of the *d*-spacing values, it can be concluded that the HDPE unit cell was slightly larger in the bulk versus that in the oriented TCL.

Estimation of the thickness of the HDPE TCL

The data for the PA6 and HDPE fractions in the oriented scattering could be used to obtain an estimate of the TCL thickness in the UDP MFC materials. From the SEM studies (Fig. 2 and Table II)), we could estimate the average visible thickness of the reinforcing fibrils in the MFC composition. Let us consider samples 1b and 3b (Fig. 2) and suppose that the fibrils are cylindrical with a PA6 core (with a diameter of $2R_1$), being uniformly coated by a coaxial TCL of HDPE, the thickness of which is given by $R_2 - R_1$. Therefore, the visible diameter of the fibril, estimated from SEM, will be $2R_2$. Figure 16 presents a schematic view of the cross sections in the two selected UDP MFCs (without and with compatibilization).

Whenever X-rays are interacting with matter, their main partners are the electrons in the studied sample. Thus, X-ray scattering is used to probe the distribution of the electron density [ρ(*r*)] inside the material. In the field of WAXS, ρ(*r*) is identical to the average electron density (ρ). For a given material or specific phase within a material, ρ is calculated as follows[32]:

$$\rho = N_A \frac{Z_M}{M_M} \rho_m \quad (1)$$

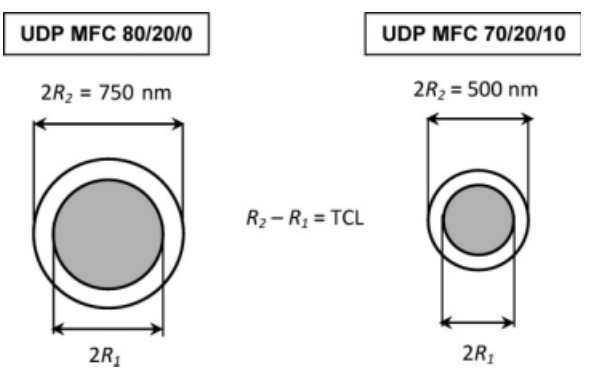

Figure 16 Schematic presentation of the fiber cross sections of 80/20/0 and 70/20/10 UDP MFCs as revealed by WAXS measurements. Both schemes are to scale.

TABLE VI
Dependence of the Structural Parameters Related to the Oriented Reinforcing Phase and the Mechanical Behavior in Various MFC Materials

	HDPE/PA6/YP	
	80/20/0	70/20/10
$2R_2$ (nm)	750	500
f	1.257	1.032
k	1.084	1.084
$2R_1$ (nm)	550	350
$R_2 - R_1$ (nm)	100	75
E_1 (MPa)	1095	920
σ_y (MPa)	57	37

where ρ_m is the average mass density, N_A is Avogadro's number (6.022×10^{23} mol^{-1}), Z_M is the number of electrons per molecule or monomer unit, and M_M is the molecular weight of the molecule or monomer unit. Therefore, the intensity of the radiation diffracted by either the PA6 phase or the HDPE phase (I_s^i) will be proportional to the volume of this phase (V_i) and the corresponding average electron density (ρ_i):

$$I_s^i \sim V_i \cdot \rho_i \tag{2}$$

If we denote the volume of the cylindrical PA6 core as V_{PA6} and the volume of the transcrystalline shell as V_{TCL}, we can write the following:

$$V_{PA6} = \pi L R_1^2 \tag{3}$$

$$V_{TCL} = \pi L (R_2^2 - R_1^2) \tag{4}$$

where L is the average length of the fibrils. Combining eq. (2) with eqs. (3) and (4), we can deduce the following simple dependence between R_2 and R_1:

$$R_1 = R_2 \cdot \sqrt{\frac{f}{k+f}} \tag{5}$$

where $k = \rho_{PA6}/\rho_{HDPE}$ and $f = I_s^{PAG}/I_s^{HDPE}$. The values of f were taken from Table V. The electron density of HDPE (ρ_{HDPE}) was found to be 347.1 eu/nm^3, and the electron density of PA6 (ρ_{PA6}) was found to be 376.2 eu/nm^3.

Table VI summarizes the structural information related to the reinforcing fibrils as revealed by the SEM and WAXS methods (i.e., $2R_1$, $2R_2$ and $R_2 - R_1$) for two MFC materials: the 80/20/0 and 70/20/10 compositions.

It can be concluded that in the HDPE/PA6/YP UDP MFCs, compatibilization resulted in thinner fibrils in which both the polyamide core and the TCL were finer. Apparently, the TCL and PA6 core thicknesses, along with the respective aspect ratios, were directly related to the mechanical performance of the composites. In the case of the PA6 reinforcement, the greater the shell and core thicknesses were, the better the mechanical properties were.

Studying the TCL in MRB and NOM composites by the reported SAXS/WAXS procedure was impossible because of the lack of a preferred orientation.

CONCLUSIONS

The microfibrillar structure of the PA6 phase in a series of HDPE/PA6/YP MFC materials with unidirectional orientation of the reinforcing fibrils was confirmed by a combination of SEM, synchrotron WAXS, and synchrotron SAXS analyses. The diameter and length of the fibrils were found to decrease as a function of the compatibilizer concentration. The X-ray analysis revealed the presence of an oriented layer of the transcrystalline matrix HDPE upon the PA6 oriented phase, suggesting a shell–core structure of the reinforcing fibrils. It was possible to estimate the real thickness of the PA6 core and the TCL in the two samples without and with compatibilization.

A direct relation was found between the mechanical properties of the HDPE/PA6/YP UDP composites and the aspect ratios of the reinforcing fibrils and their core and shell thicknesses. Comparing the mechanical properties of the UDP, MRB, and NOM materials, we showed that the fibrous reinforcement enhanced the strength of the matrix. Thus, all the HDPE/PA6/YP MFCs with uniaxially aligned PA6 reinforcing fibrils showed better longitudinal tensile characteristics than HDPE, the improvement being up to 33% for the secant modulus and up to 120% for the tensile strength. The composites with the highest concentration of the compatibilizer showed the smallest enhancement of the tensile properties.

References

1. Evstatiev, M.; Fakirov, S. Polymer 1992, 33, 877.
2. Evstatiev, M.; Fakirov, S.; Schultz, J. M. Polymer 1993, 34, 4669.
3. Evstatiev, M.; Fakirov, S.; Friedrich, K. Appl Compos Mater 1995, 2, 93.
4. Fakirov, S.; Evstatiev, M.; Friedrich, K. In Handbook of Thermoplastic Polyesters; Wiley-VCH: Weinheim, 2002.
5. Newnham, R. E.; Giniewicz, J. R. Comprehensive Composite Materials; Elsevier: Amsterdam, 2000; Vol. 1.
6. Denchev, Z.; Dencheva, N. Polym Int 2008, 57, 11.
7. Fakirov, S.; Evstatiev, M.; Petrovich, S. Macromolecules 1993, 26, 5219.
8. Apostolov, A. A.; Evstatiev, M.; Fakirov, S.; Kloczkowski, A.; Mark, J. E. J Appl Polym Sci 1996, 59, 1667.
9. Evstatiev, M.; Schultz, J. M.; Petrovich, S.; Georgiev, G.; Fakirov, S.; Friedrich, K. J Appl Polym Sci 1998, 67, 723.
10. Sapoundjieva, D.; Denchev, Z.; Evstatiev, M.; Fakirov, S.; Stribeck, N.; Stamm, M. J Mater Sci 1999, 34, 3063.
11. Fakirov, S.; Evstatiev, M. Adv Mater 1994, 6, 395.

12. Evstatiev, M.; Fakirov, S.; Bechtold, G.; Friedrich, K. Adv Polym Technol 2000, 19, 249.
13. Fakirov, S.; Kamo, H.; Estatiev, M.; Friedrich, K. J Macromol Sci Phys 2005, 43, 775.
14. Friedrich, K.; Evstatiev, M.; Fakirov, S.; Evstatiev, O.; Ishii, M.; Harrass, M. Compos Sci Technol 2005, 65, 107.
15. Monticciolo, A.; Cassagnau, P.; Michel, A. Polym Eng Sci 1998, 38, 1882.
16. Pesneau, I.; Ait-Kadi, A.; Bousmina, M.; Cassagnau, P.; Michel, A. Polym Eng Sci 2002, 42, 1990.
17. Evstatiev, M.; Fakirov, S.; Krasteva, B.; Friedrich, K.; Covas, J. A.; Cunha, A. M. Polym Eng Sci 2002, 42, 826.
18. Li, Z. M.; Yang, M. B.; Huang, R.; Yang, W.; Feng, J. M. Polym Plast Technol Eng 2002, 41, 19.
19. Li, Z. M.; Yang, W.; Xie, B. H.; Shen, K. Z.; Huang, R.; Yang, M. B. Macromol Mater Eng 2004, 289, 349.
20. Li, Z. M.; Xie, B. H.; Huang, R.; Fang, X. P.; Yang, M. B. Polym Eng Sci 2004, 44, 2165.
21. Li, Z. M.; Li, B. L.; Shen, K. Z.; Yang, W.; Huang, R.; Yang, M. B. Macromol Rapid Commun 2004, 25, 553.
22. Fuchs, C.; Bhattacharyya, D.; Fakirov, S. Compos Sci Technol 2006, 66, 3161.
23. Denchev, Z.; Oliveira, M. J.; Carneiro, O. S. J Macromol Sci Phys 2004, 43, 143.
24. Dencheva, N.; Oliveira, M. J.; Carneiro, O. S.; Nunes, T. G.; Denchev, Z. Mater Sci Forum 2008, 587, 515.
25. van Duin, M.; Aussems, M.; Borggreve, R. J. M. J Polym Sci Part A: Polym Chem 1998, 36, 179.
26. Thomas, S.; Groeninckx, G. Polymer 1999, 40, 5799.
27. Powell, P. C. Engineering with Fiber–Polymer Laminates; Chapman & Hall: London, 1994; p 23.
28. Palabiyik, M.; Bahadur, S. Wear 2000, 246, 149.
29. Dencheva, N.; Nunes, T. G.; Oliveira, M. J.; Denchev, Z. Polymer 2005, 46, 887.
30. Nogales, A.; Hsiao, B. S.; Somani, R. H.; Srinivas, S.; Tsou, A. H.; Balta-Calleja, F. J.; Ezquerra, T. A. Polymer 2001, 42, 5247.
31. Polar Software, Version 2.7.1; Stonybrook Technology and Applied Research: New York, 2008.
32. Stribeck, N. X-Ray Scattering of Soft Matter; Springer-Verlag: Berlin, 2007; p 42.